



The Role of Nanocrystallization for the Enhancement of Structural, Electrical, and Transport Properties of BaTiO₃-V₂O₅-PbO Glasses

Ibrahim Morad¹ · Amany E. Harby¹ · M. S. Ayoub¹ · H. Elhosiny Ali² · M. M. El-Desoky¹

Received: 24 April 2023 / Accepted: 25 July 2023
© The Author(s) 2023

Abstract

Glass-ceramic nanocrystals (GCNs) were created via annealing at crystallization temperature T_c for the parent BaTiO₃-V₂O₅-PbO glasses prepared by the melt quenching technique. The amorphous character of the existing quenched glasses was confirmed by scanning electron microscopy. Furthermore, the general characteristics of x-ray diffraction support the amorphous nature of the glasses. In the related heat-treated samples, the typical nanostructure size is less than 60 nm. It was discovered that an increase in the density of the GCNs occurred with an increase in the BaTiO₃ percentage. Also, with increasing BaTiO₃ content, a slight increase was observed in the crystallization and glass transition temperature from 335°C to 365°C and 265°C to 320°C, respectively. It was revealed that suitable nanocrystallization at temperatures around the onset of T_c for 1 h was able to significantly increase the electronic conductivity of the initial glasses. The accumulation of V⁴⁺-V⁵⁺ pairs at the interlayer zones created between nanocrystallites and the glassy phase were accountable for electron hopping in the current approach, which was significantly higher than in the glass phase. The experimental findings were investigated in a model based on the “core-shell” idea. Appropriate values for the different small polaron hopping (SPH) variables were found from the best fits. Non-adiabatic hopping of small polarons was responsible for the conduction. As a result of the alteration of the nanostructure, conductivity was enhanced. Compared to the original glasses, the final materials have significantly better electrical conductivity. Such characteristics can be utilized in the design for industrial applications.

Keywords DC conductivity · glass-ceramic · nanocomposites · SPH

Introduction

A critical issue for nanotechnology advancement is the creation of nanocrystals. Several techniques for creating nanocrystals have been investigated, including the solid reaction approach,¹ sol-gel method,² hydrothermal method,³ aerosol method,⁴ and the growth and nucleation mechanism while heating glass.⁵ Each technique, however, has drawbacks and restrictions. A solid reaction process, for instance, necessitates a high temperature and a protracted reaction period. In addition, mainly submicron or micron-sized

particles can develop, and throughout their post-treatments, including the milling procedure, contaminants may be added.⁵ Glass-ceramic nanocrystals (GCNs) are created by annealing glasses at temperatures around the crystallization temperature.^{5–10} The physical characteristics of GCNs, which are not found in other glass material, make them significant. A wide variety of types and sizes of crystals can be used to make GCNs (nano, micro, etc.). The mobility of the electrons is significantly impeded by a grain barrier. This is because the orientation of the crystal lattice with respect to the entering electron's wave vector differs on either side of the grain boundary,¹¹ and as a result, the electron will always experience an important scattering event whenever it comes into contact with a grain boundary. Consequently, the resistivity of a crystalline material increases with decreasing grain size because there are more grain boundaries present.¹² Therefore, we can conclude that the most important structural factors in electronic nanocrystalline glassy states are crystal and grain size.^{7,13}

✉ Ibrahim Morad
imorad@zju.edu.cn

✉ M. M. El-Desoky
mmdesoky@suezuniv.edu.eg

¹ Department of Physics, Faculty of Science, Suez University, Suez 43518, Egypt

² Department of Physics, Faculty of Science, Zagazig University, Zagazig, Egypt

Substantial quantities of ferroelectric material with varying dielectric characteristics and forms are needed for various electrical applications. In microwave furnaces,¹⁴ which demand adjustable dielectric permittivity throughout a wide range and with minimal dielectric losses, such materials could be employed to regulate and homogenize fields. The study of the ferroelectric properties of BaTiO₃ in a glassy matrix or glass ceramics as nanocrystals, which are appealing for pyro-electric, piezoelectric, and electro-optic applications, is becoming increasingly popular. Recently, it was discovered¹⁵ that ferroelectricity can occur in a glassy structure comprising transition metal oxides (TMO), such as glass based on Bi₂O₃-CuO-Pb₂O₃. Additionally, certain TMO glasses with BaTiO₃, LiTiO₃, NaNbO₃, PbTiO₃, etc., form homogeneous glasses with V₂O₅-PbO, V₂O₅-Bi₂O₃, and V₂O₅-P₂O₅.

The optimum electronic conductors in a V₂O₅-containing system are glasses and GCNs.^{16,17} They are frequently used as a model for an electrical conductor because they acquire certain structural characteristics and transport properties from the nanocrystalline phases of V₂O₅, particularly from its phase.¹³ Nonetheless, it has recently been proven that obtaining fine-grained exogenous phases evenly dispersed inside matrices with intermediate conductivity (glass, polymer electrolytes, or polycrystalline solids) can significantly increase the conductivity of those materials.^{13,14,17,18}

Because of their semiconducting nature, TMO-rich oxide glasses and related GCNs exhibit intriguing electronic characteristics.^{5,19,20} This is due to the following: (1) TMOs have a diverse range of constituent elements and can accommodate a wide range of defects, including interstitial defects, local structural distortions, grain boundaries, domain walls, misfit dislocations, oxygen vacancies (VO), cation vacancies (VC), and impurities such as H⁺/Li⁺; and (2) TMOs have many constituent elements. Because TMOs are ionic, defects tend to have high transition energies and additional localized charges, which means that defects in TMOs typically do not significantly alter electrical conductivity as they do in conventional semiconductors.²¹ At elevated temperatures and owing to redox reactions accumulating in the melt during processing, transition metal ions exist in two separate valence states inside the glass network simultaneously, which greatly influences this behavior.

Between the two vanadium ions in the glass, V⁴⁺ → V⁵⁺ + e occurs during the conduction of V₂O₅-containing glass modifications. This charge transfer is often referred to as “small polaron hopping” (SPH).^{22,23} The electrical conductivity of these glasses is highly dependent on the regional interactions between an electron's surroundings and the spacing separating vanadium ions.^{13,14,18,20}

Our previous work²⁴ investigated the nanostructure and electrical properties of a BaTiO₃-V₂O₅ glass system and its corresponding GCNs. Transmission electron microscopy

(TEM) and x-ray diffraction (XRD) of the present GCNs indicated nanocrystals with a particle size of 20–35 nm. The GCN conductivity was indeed found to be greater compared to the related glassy phase. This enhanced GCN conductivity was believed to be a consequence of the existence of the nanocrystal as a result of the extensive network development of electronic conduction channels that were located within and on the V₂O₅ surface nanocrystals. It was fascinating to observe that, as expected from the observations of the dielectric permittivity, the pure nanocrystalline BaTiO₃ phase with an average particle size of less than 100 nm also exhibits its ferroelectric phase transition around this temperature. By appropriately adjusting annealing time and BaTiO₃ content, such GCNs may be employed to modulate BaTiO₃ particle size and, consequently, transition temperature. Such a quality applies to industrial applications in which the material structure is crucial.

Investigating the glass system of xBaTiO₃-(80-x)V₂O₅-20PbO (*x* have values of 5 mol.%, 10 mol.%, 15 mol.%, 20 mol.%, and 25 mol.%) is the primary goal of the current work. Our study involves three main issues: firstly, the preparation of the glass and GCNs; secondly, exploring how Mott's SPH model affects the nanostructural compositional dependency and V₂O₅ transport properties of GCNs,^{22,23} and lastly, elucidating the mechanism of electrical conductivity in BaTiO₃-V₂O₅-PbO glasses and related GCNs, produced by annealing for 1 h around the crystallization temperature.

Experimental Technique

Sample Preparation

GCNs of xBaTiO₃-(80-x)V₂O₅-20PbO (where *x* = 5 mol.%, 10 mol.%, 15 mol.%, 20 mol.%, and 25 mol.%) were formed during heat treatment of conventional melt quenching glasses. High-purity powders of BaTiO₃ (99.5%), V₂O₅ (99%), and PbO (99.9%), all obtained from Sigma-Aldrich, were our starting chemicals, with a total mixture of 10 g weighed in a stoichiometric ratio. The mixture was ground until homogeneous in an agate mortar in a wetting medium of acetone. The mixture was placed in a porcelain crucible and melted at 1100°C for 1 h according to the composition in a high-temperature furnace. The melt was then quenched onto a stainless-steel plate and instantly pressed to obtain uniform-thickness glass samples. An additional 2 h of annealing at 350°C is performed to reduce the internal stresses produced during thermal treatment. Finally, we obtained a transparent glass plate with a uniform thickness of 1.6 mm and a diameter of 2.5–3.0 cm. For the formation of GCNs, the resulting glass was heated in air at crystallization temperature for 1 h.

Sample Characterization

To determine the glassy nature of our system, the thermal properties of the as-melted glasses were examined by differential thermal analysis (DTA) at a heating rate of $10^{\circ}\text{C}/\text{min}$ from room temperature to 800°C using a Shimadzu DSC-50 differential scanning calorimeter (DSC). Archimedes' principle was used to calculate the densities of G and GCNs using the standard relation $\rho = (W_a / W_a - W_L) \rho_L$, where W_a , W_L , and ρ_L are the sample weight in the air, toluene, and the density of toluene. The G and GCNs were subjected to XRD analysis using a Bruker D8 Advance diffractometer with Cu-K α radiation (1.54 \AA). XRD analysis was performed under operating conditions of tube voltage & current of 40 kV & 40 mA , respectively, and scanning speed of 0.02 sec^{-1} , in the range between 10° and 80° . The heat-treated GCNs were subjected to selected-area electron diffraction (SAED) examinations to determine and identify the crystallites ingrained in the glass matrix. A high-resolution transmission electron microscope (JEOL JEM-200 CX) was utilized to analyze the crystallinity of the granules of the GCNs.

Setup of Electrical Conductivity

The DC conductivity (σ) of the proposed system was evaluated between ambient temperature and 475 K . A unique measurement device and a furnace were created, both of which can achieve temperatures of up to 500°C . To achieve the DC measurements, the glass samples were shaped to a regular shape with a specific area and thickness; in addition, the faces of both samples were polished with a silver paste to construct an electrode. After that, the DC data were measured at temperatures between 310 K and 450 K using a Keithley 485 picoammeter by establishing the I - V trend across electrodes.

Results and Discussion

Structural Behavior

DSC

For the current glass matrix, the compositional dependency of the glass transition temperature (T_g), crystallization temperature (T_c), and melting temperature (T_m) is shown in Fig. 1 together with the DSC thermogram for the BaTiO_3 - V_2O_5 - PbO glasses. The endothermic decline,

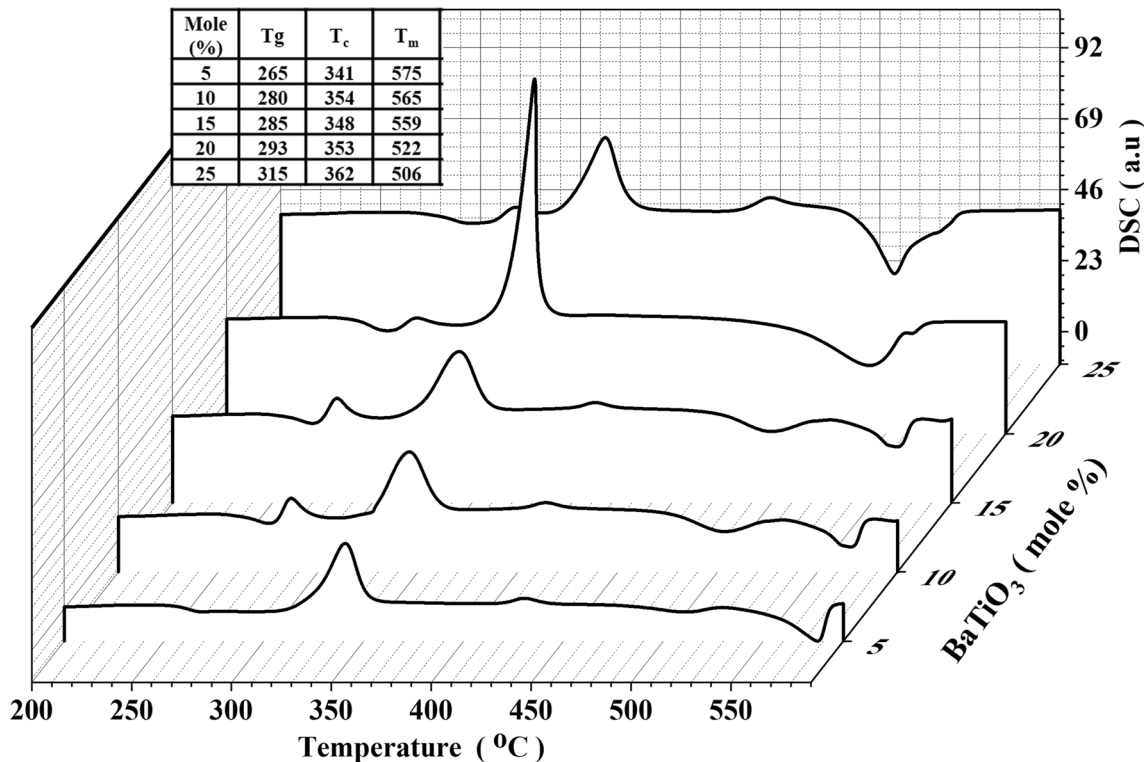


Fig. 1 DSC thermogram for BaTiO_3 - V_2O_5 - PbO glasses glass and composition dependence of glass transition temperature (T_g), crystallization temperature (T_c), and melting temperature (T_m) for different glass compositions.

which corresponds to T_g , is identified roughly from 254°C to 276°C. However, crystallization is indicated by the exothermic peak (T_c) in the temperature range of 325–363°C. Moreover, between 490°C and 535°C, endothermic decline is caused by the melting temperature (T_m). The glass transition temperature (T_g) shifts to higher temperatures by increasing BaTiO_3 content, which implies the reduction of the influence of non-bridging oxygen (NBO). By increasing BaTiO_3 content, the crystallization temperature (T_c) increases almost linearly.²⁴ In contrast, the DSC analysis of the structures of numerous glasses has indeed demonstrated the formation of NBO atoms and the strong association between T_g and the alteration of the network former's coordination number, which indicates the breakdown of the network structure.²⁵ T_g often displays a tremendous increase as the network former's coordination number increases. Contrarily, the growth of NBO results in a reduction in T_g . Thus, the steady rise in T_g in the current system seems to indicate that the ratio of V^{5+} and V^{4+} ions that can coordinate is continuing to decline and that NBO atoms are being destroyed.²⁶

XRD

Figure 2 displays exemplary XRD patterns of (a) BaTiO_3 - V_2O_5 - PbO glasses and (b) associated GCNs. No sign of diffraction peaks is observed, only a broad halo that supports the original glasses' amorphous state theory. The samples were heated for a full hour at the crystallization temperature. While there continues to be a sizable amount of material in the amorphous phase, several peaks appear that belong to nanocrystalline phases overlaid on a broad halo. The XRD pattern of the heat-treated sample demonstrates that heating around T_c only starts to result in tiny nanocrystallites in the glass network.^{13,14,18} This can help to control the number of nanocrystalline phases inside the material and modify the electrical conductivity by altering the annealing time and temperature. The phases identified as nanocrystalline included $\text{Ba}_3\text{TiV}_4\text{O}_{15}$, BaTiO_3 , V_2O_5 , and PbO . Furthermore, certain additional peaks are associated with phases that still have not been located. The average size of the nanocrystallites may be obtained from the widths of the diffraction peaks to a maximum of 50 nm using the Scherrer formula. BaTiO_3 and V_2O_5 nanocrystallites with an average size of 40–60 nm were calculated from x-ray line-broadening measurements.

Transmission Electron Microscopy (TEM)

As an example, the TEM micrograph and SAED pattern of the 20 BaTiO_3 -60 V_2O_5 -20 PbO glass sample are presented in Fig. 3a.

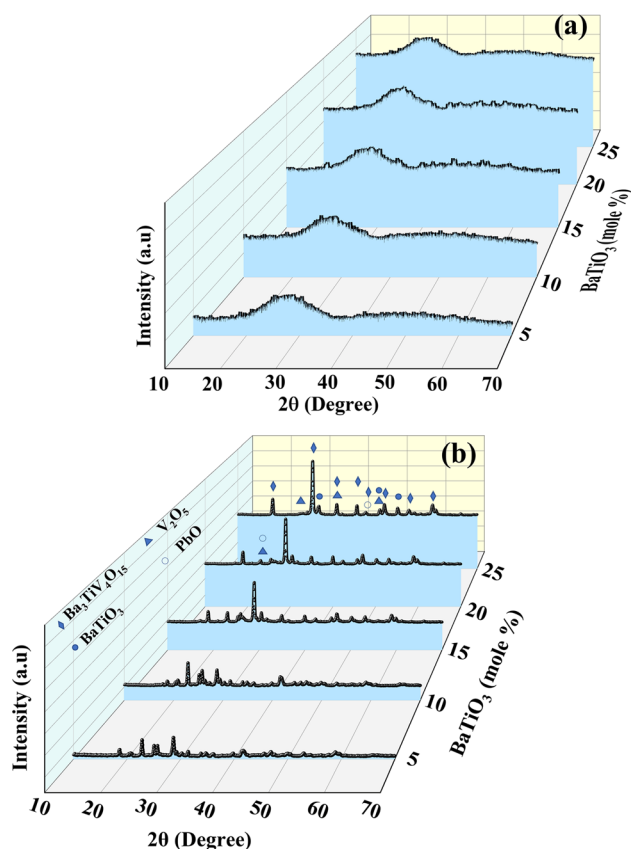


Fig. 2 X-ray diffraction for (a) BaTiO_3 - V_2O_5 - PbO glasses and (b) GCNs.

The amorphous phase is confirmed by the SAED pattern, which is displayed as an inset. So far, a distinct halo in this pattern shows that the sample is related to some degree of crystallinity. The electron microscopy (Fig. 2) taken for the sample that was heated to the crystallization temperature for 1 h indicates the existence of nearly spherical particles that are uniformly disseminated in a glass matrix and are of relatively consistent size, assessed between 40 nm and 50 nm. The involvement of BaTiO_3 and V_2O_5 nanocrystallites is confirmed by the SAED pattern (inset of Fig. 3b) and the lattice spacing's 'd' throughout. Such sample's SAED profile which is represented in the inset of Fig. 3b exhibits a glassy halo, which could be explained by the strong diffraction of the glassy matrix, which hides the diffraction from crystalline nuclei.⁵ Similar outcomes have been attained with the other samples. According to TEM examinations, nanoparticles with a grain size of 40–50 nm are almost homogeneous yet moderately agglomerated (Fig. 3b).

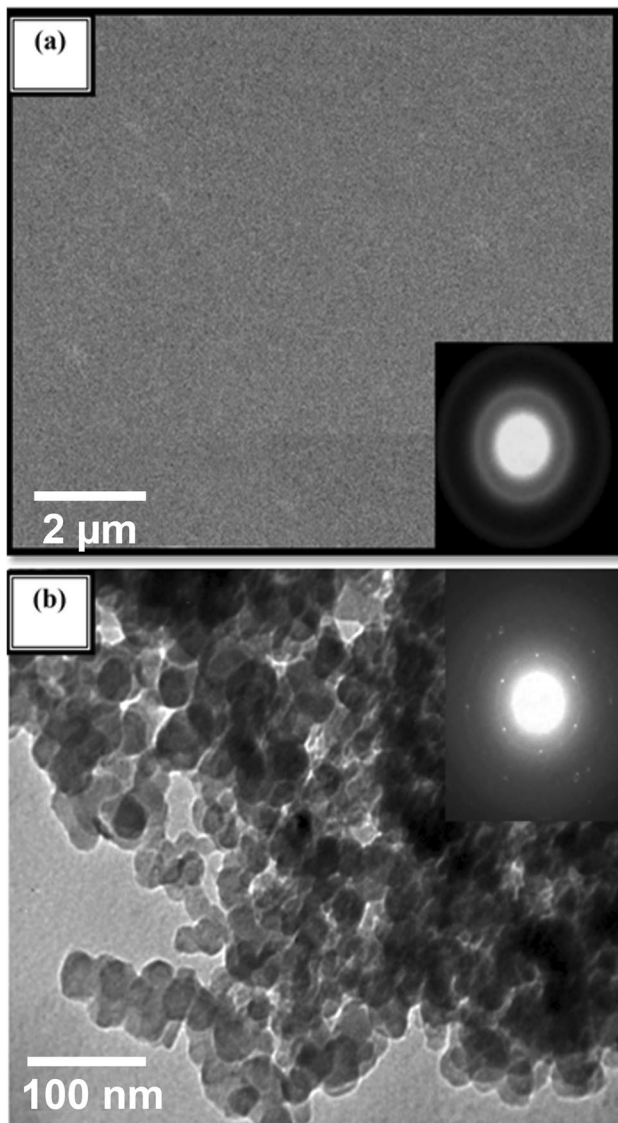


Fig. 3 TEM and selected area electron diffraction (inset) for (a) 20BaTiO₃-60V₂O₅-20PbO glass and (b) GCN.

Density

Figure 4 displays densities (d) for glasses and associated GCNs as a function of BaTiO₃ content. With the increase in the BaTiO₃ level, the density appears to steadily increase. The density data demonstrate that by increasing Ti cation concentration, the structure of the glasses and related GCNs is slightly open, permitting the potential creation of a declining number of NBO.²⁵ Here, the current system, the densities for glasses and the GCNs range from 4.03 g/cm³ to 5.85 g/cm³ and 4.3 g/cm³ to 6.16 g/cm³, respectively, as presented in Tables I and II. The increasing of glass composition glass with contents was also deduced by Mahmoud et al.,²⁷ the demonstrated density of the 80B₂O₃-(20-x) Na₂O-x CdO

glasses increases as the cadmium content increases, varying between 2.19 g cm⁻³ and 2.89 g cm⁻³

DC Conductivity

Conductivity and Activation Energy

Figure 5a and b illustrate the logarithm of the DC conductivity of the current glasses and associated GCNs, respectively, as a proportion of the inverse temperature. The graph illustrates the linear relationship between temperature and quantity up to a temperature of $\theta_D/2$ (θ_D Debye temperature). That behavior results from the transitions across mixed valence states of electrons or polarons.^{13,17,18}

To fit the empirical conductivity data beyond $\theta_D/2$, Mott's small polaron hopping (SPH) theory was used.^{22,23} The slope of each graph in the highest range of the temperature recorded was used to calculate the high-temperature activation energy. The activation energy on behalf of conduction provided by the Mott formula accurately describes the experimental conductivity measurements in such a condition.^{22,23,28}

$$\sigma = \sigma_o e^{-\frac{W}{kT}} \quad (1)$$

where W is the activation energy, k is the Boltzmann constant, and σ_o is a pre-exponential variable. In Fig. 6, it is depicted how the high-temperature conductivity and high-temperature activation energy of glasses and associated GCNs vary with concentration. With the increase in BaTiO₃ content, the conductivity drops while activation energy rises, as shown in the figure. This behavior is a characteristic of SPH.^{26,29-31} In the situation where the electrical conductivity is low and the activation energy is large, comparable to the properties of the BaTiO₃-V₂O₅ and SrTiO₃-V₂O₅-PbO₂ glasses.^{5,24} As BaTiO₃ content rises and the V₂O₅ level falls, there could be structural alterations that are occurring confined by this shift in conductivity and activation energy.

Figure 6 shows how the conductivity of glasses and related GCNs varies with BaTiO₃ concentration at a constant temperature (373 K). The fact that all these associated GCNs display high conductivity compared to the samples in the glassy phase is intriguing to remark.²⁴ According to TEM and XRD studies, the enhanced conductivity of these related GCNs is caused by the existence of nanocrystals with an average particle size of 40–60 nm. Other BaTiO₃-V₂O₅ and SrTiO₃-V₂O₅-PbO₂ glasses have also been reported to demonstrate such high conductivity enhancements. At high temperatures, the conduction activation energy was determined to be $W_{GCNs} = 0.20-0.27$ eV, which seems to be markedly smaller in comparison to the as-prepared glasses $W_g = 0.34-0.47$ eV at elevated temperatures (Tables I and II). Our result is comparable to that deduced by Ibrahim,³²

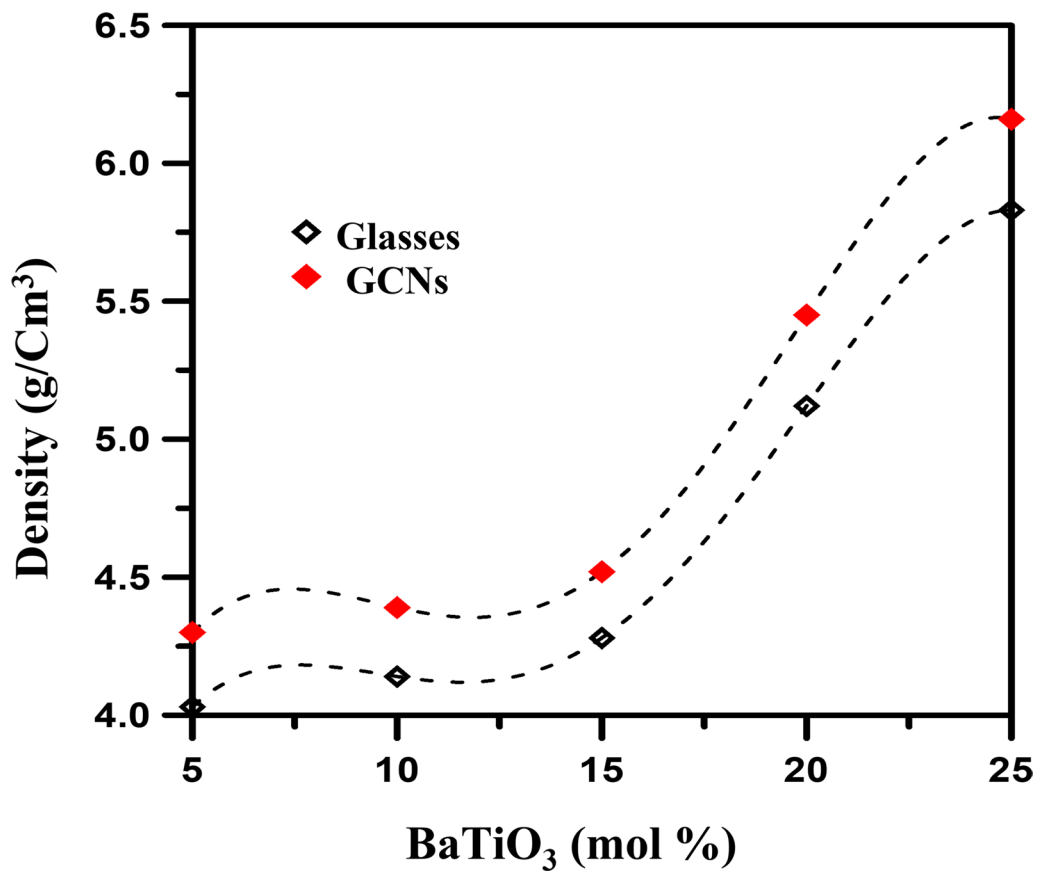


Fig. 4 Variation of density (d) with the different BaTiO₃ for BVP glasses and GCNs.

Table I Several significant BaTiO₃-V₂O₅-PbO glass physical characteristics and SPH parameters

Nominal composition (mol%)			D ±0.02 (g cm ⁻³)	W _g ±0.01 (eV)	R ±0.01 (nm)	N ±0.01 (× 10 ²² cm ⁻³)	r _p ±0.001 (nm)	θ _D ±1 (K)	ν _o ± 0.01 (× 10 ¹³ Hz)	N(E _F) (× 10 ²²) (eV ⁻¹ cm ⁻³)
BaTiO ₃	V ₂ O ₅	PbO								
5	75	20	4.03	0.34	0.469	0.97	0.189	615	1.27	0.68
10	70	20	4.14	0.36	0.265	5.35	0.106	625	1.30	3.56
15	65	20	4.28	0.38	0.235	7.68	0.094	630	1.31	4.87
20	60	20	5.12	0.39	0.216	9.83	0.087	635	1.32	6.12
25	55	20	5.83	0.41	0.203	11.8	0.082	645	1.34	6.96

Table II Some important physical properties and SPH parameters of BaTiO₃-V₂O₅-PbO glass-ceramic nanocrystals

Nominal composition (mol%)			d ±0.02 (g cm ⁻³)	W _{GCNs} ±0.01 (eV)	R ±0.01 (nm)	N ±0.01 (× 10 ²² cm ⁻³)	r _p ±0.001 (nm)	θ _D ±1 (K)	ν _o ± 0.01 (× 10 ¹³ Hz)	N(E _F) (× 10 ²²) (eV ⁻¹ cm ⁻³)
BaTiO ₃	V ₂ O ₅	PbO								
5	75	20	4.03	0.20	0.50	1.03	0.202	581	1.20	0.40
10	70	20	4.14	0.21	0.28	5.67	0.111	588	1.22	2.08
15	65	20	4.28	0.24	0.25	8.11	0.103	594	1.24	3.08
20	60	20	5.12	0.26	0.23	10.46	0.092	599	1.26	4.08
25	55	20	5.83	0.27	0.21	12.46	0.864	605	1.26	4.63

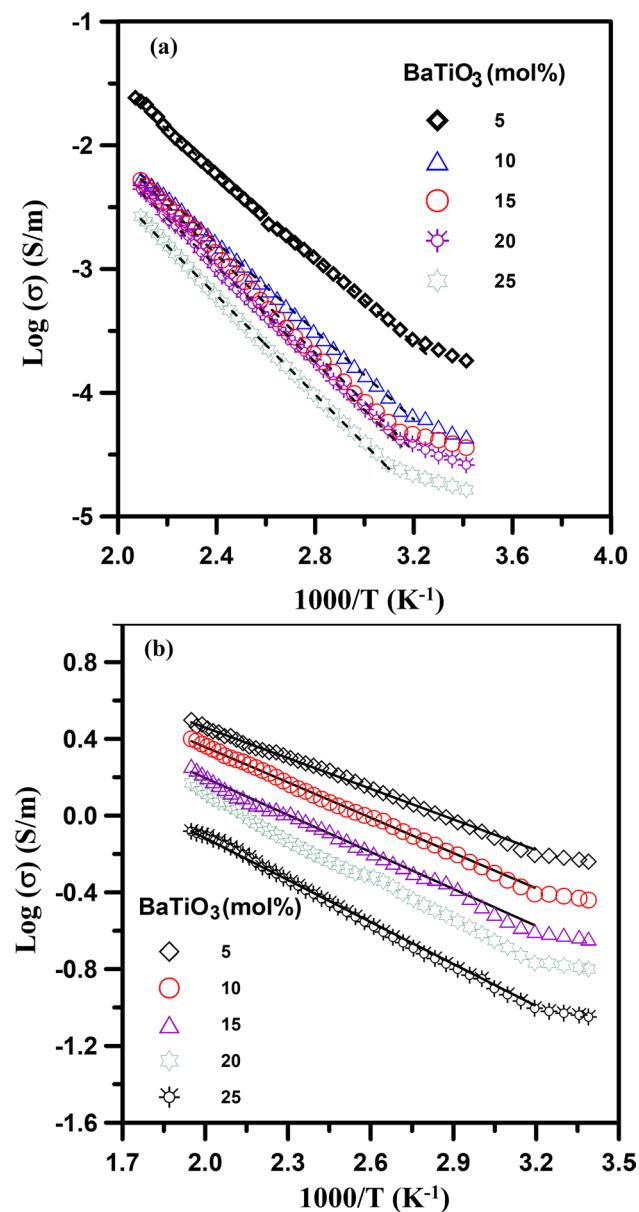


Fig. 5 Arrhenius plots on account of BaTiO_3 content for (a) glasses and (b) GCNs.

who found activation energy of 0.23–0.31 eV for glasses and 0.19–0.23 eV for the GCNs. This suggests a decrease in activation energy W and an increase in σ due to an increase in the V^{4+} ion fraction (Fig. 6). The BaTiO_3 addition lowered the conductivity in the $\text{BaTiO}_3\text{-V}_2\text{O}_5\text{-PbO}$ system in our current study (Fig. 5). In particular, it is understood that the reduction in NBO cations caused by the addition of BaTiO_3 to glass reduces conductivity.²⁴ This might reduce the open structure, which would allow for less mobility for the charge carriers. This outcome is in accord with findings regarding density (as referred to in Fig. 4).

On the contrary, the following explains how the electrical conductivity of the GCN system under study improved. The distribution pattern of V^{4+} and V^{5+} ions seems to suggest sites of electron hopping in the glass system, in which a substantial proportion of V_2O_5 is particularly crucial for electronic conduction.^{13,14,16,24} There is a haphazard arrangement of all these centers throughout the initial glass. The development of nanocrystalline V_2O_5 crystallites embedded in the glass matrix results from annealing at temperatures near the crystallization temperature. The boundary across crystalline and amorphous aspects is very substantially ramified and greatly affects the whole electrical characteristics of the nanocomposites as described by TEM and XRD because the average particle size is minimal, roughly 40–60 nm. It might have more concentrated V^{4+} and V^{5+} centers distributed across the V_2O_5 crystallite surface.^{13,14,16,24} Nevertheless, such an increase in electrical conductivity is thought to be due to (i) an increase in $\text{V}^{4+}\text{-V}^{5+}$ pair concentration (possibly clarifying this increase among both nanocrystalline surfaces and the glassy stage), and (ii) the defective emergence, well-conducting zones beside the glass–crystallite interfaces.^{13,14,16,24}

Also, the increased activation energy and decreased DC conductivity of the current samples point to certain modifications in the conduction pathways. Scientists have previously observed that in glasses incorporating V_2O_5 , the DC conductivity shows electronic behavior and varies substantially according to the average distance, R , between the V-ions.^{19,20,25,26,29,30} The mean distance, R , has been estimated for the current system according to the equation $R = (1/N)^{1/3}$, in which N represents V-ion concentration per unit volume determined by the batch composition and observed density (Tables I and II).

For the glasses and related GCN systems, the density, d , V-ion content per volume, N , and mean separation, R , are provided in Tables I and II, respectively. The mean separation (R) and activation energy (W) between glasses and GCNs are depicted in Fig. 7. These findings are in agreement with those made by El-Desoky,^{5,24} who established the relationship between W and the site distance of V-O-V. Meanwhile, in our situation, one could anticipate that the proportion of $\text{V}^{4+}\text{-V}^{5+}$ pairs has outdistanced the surfaces of the freshly created crystalline phase compared to the residual amorphous phase as well as within crystallites as a result of the nanocrystal growth.^{5,24} It is well recognized that the imperfect state of the interfaces between the crystalline and amorphous states is the source of several significant characteristics of nanomaterials.¹⁹ Based on the Mott theory,^{5,24} a high $\text{V}^{4+}\text{-V}^{5+}$ pairing content results in a shorter average distance between the hopping centers and an enhancement in conductivity. Higher-than-average conductivity interface portions serve as a sort of “smooth conduction path” intended for electrons.^{5,13,14,18,33} A theory for the increase

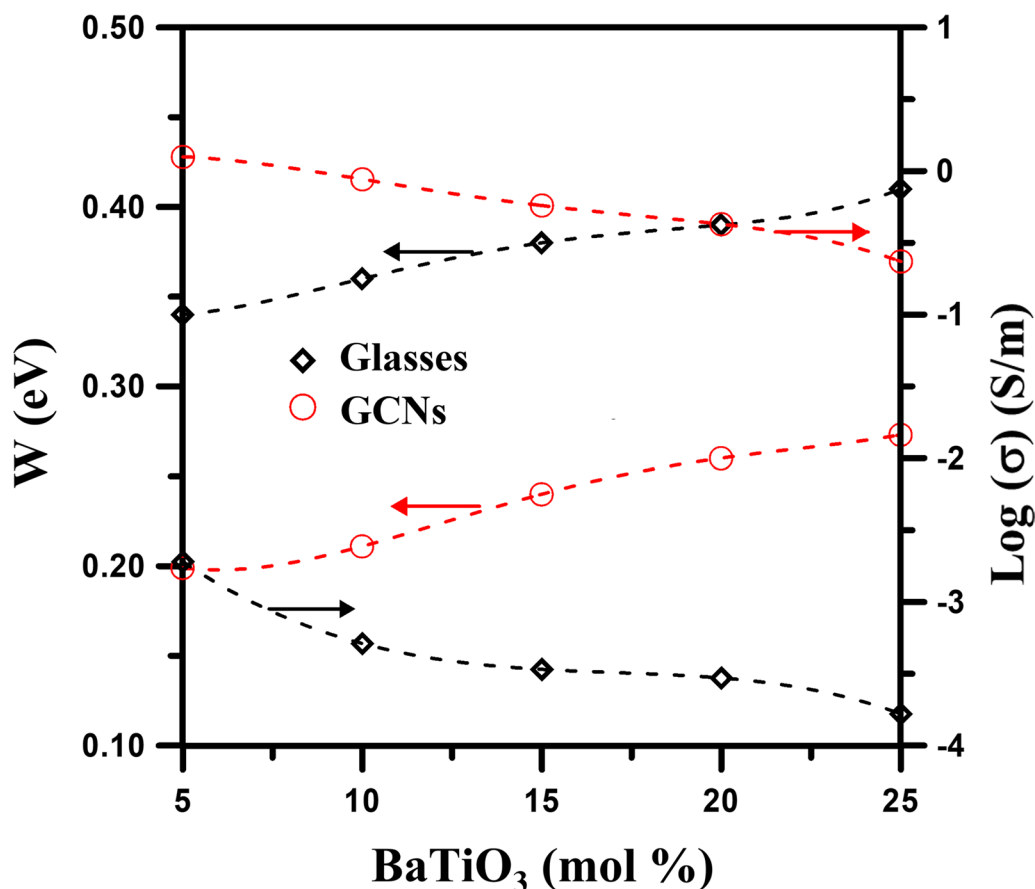


Fig. 6 The dependence of conductivity and activation energy on BaTiO₃ ratios for glasses and GCNs.

in conductivity brought on by nanocrystallization has been described by Pietrzak et al.³⁴

Nevertheless, in this instance, it appears from the TEM and conductivity results that a crystalline portion of the grain (as shown from the XRD pattern) is surrounded by a severely deformed or indeed amorphous part. TEM micrographs show the entire grain, including its deformed outer layer and crystalline inner layer. This explanation is consistent with the “core–shell” model of the nanosized grains found in materials that have undergone thermal nanocrystallization, like the one being studied. This theory states that grain is made up of an exterior, extremely disordered, faulty, and non-stoichiometric “shell” and an inner, totally crystalline “core”.³⁴ The increase in conductivity brought on by nanocrystallization can be explained by the same “core–shell” idea. The representation of such a model was graphically represented as a schematic diagram by El Desoky et al. and Pietrzak.^{34,35} Defective shells that surround crystalline cores can merge and cross over, creating a complex network of pathways for enhanced electron transport. The tiny polaron hopping between the V⁴⁺ and V⁵⁺ sites provides the basis for the electronic transport

mechanism in vanadium oxides. In areas where the local V⁴⁺–V⁵⁺ pair concentration is higher, the conductivity is also higher. This situation occurs within and surrounding the damaged grain-shell regions. Due to the establishment of a vast and extensive network of electronic conduction channels that are located between iron nanocrystals and on their surfaces, a considerable improvement in electrical conductivity is observed after nanocrystallization.^{13,14,18,24}

Conduction Mechanism

Mott provided a theory for conduction processes for TMOs.²³ In this paradigm, the conduction process is viewed as the hopping of tiny polarons between localized states with the assistance of phonons. For the closest neighbors hopping in the non-adiabatic domain at high temperatures $T > \theta_D/2$, the DC conductivity in the Mott model can be estimated by^{22,23}

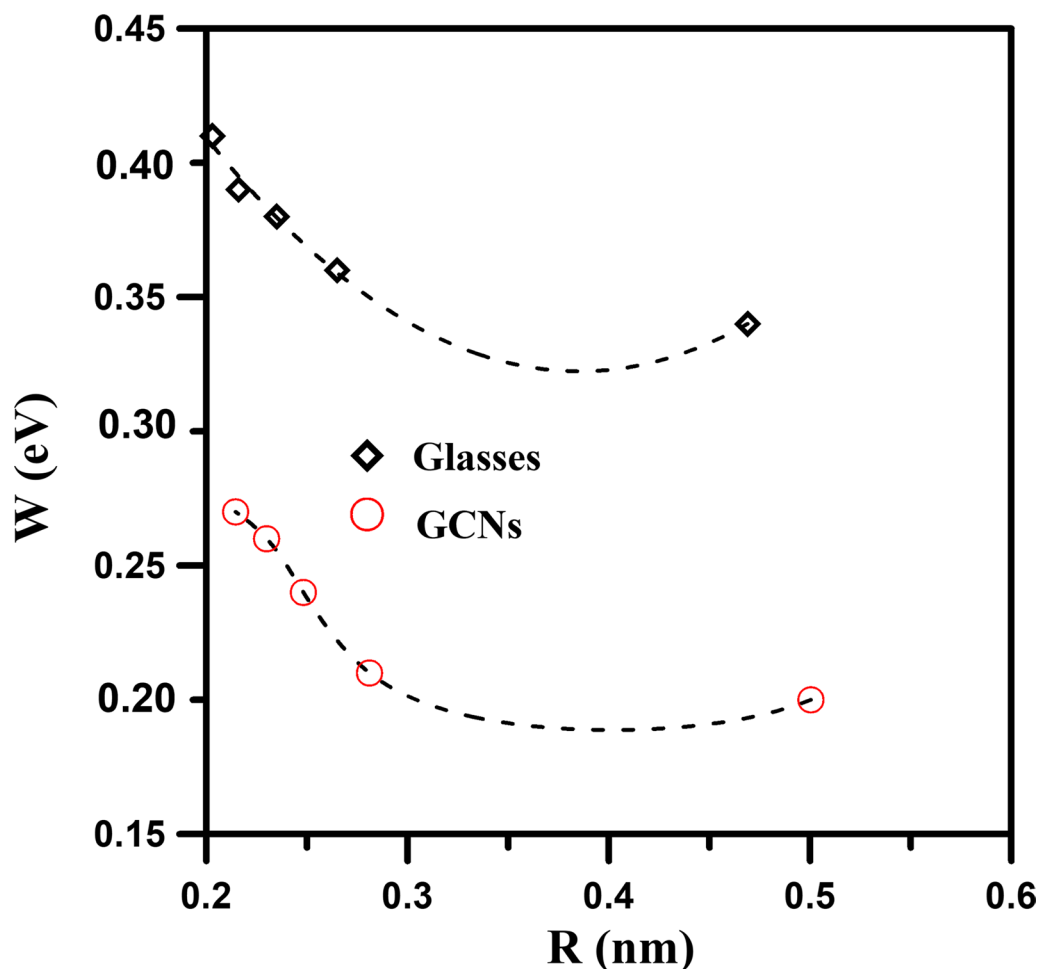


Fig. 7 The average distance (R) as a function of activation energy (W) for different glasses and GCNs.

$$\sigma = \frac{\nu_o N e^2 R^2}{kT} C(1 - C) \exp(-2\alpha R) \exp(-W/kT) \tag{2}$$

$$= \sigma_o \exp(-W/kT)$$

The pre-exponential factor (σ_o) in Eq. 2 is given by

$$\sigma_o = \frac{\nu_o N e^2 R^2}{kT} C(1 - C) \exp(-2\alpha R) \tag{3}$$

where C is the percentage of decreased transition metal ion, α is the tunneling parameter (the percentage of wave function decay), and ν_o is the optical phonon frequency. Austin and Mott²³ demonstrated that under the assumption of a robust electron-phonon interaction

$$W = W_H + W_D/2 \quad (\text{for } T > \theta_D/2) \tag{4a}$$

$$W = W_D \quad (\text{for } T < \theta_D/4) \tag{4b}$$

wherein W_D is the potential energy difference between the beginning and ending sites caused by variations in

the regional configurations of ions, and W_H is the polaron hopping energy. A graph of the conductivity logarithm versus activation energy at a constant experimental temperature T could be utilized to determine the mechanism (adiabatic/non-adiabatic) of polaron hopping for glass and GCNs.^{19,26,30} If the estimated temperature T_e , from the slope of this kind of graph, is close to the empirical temperature T , it is anticipated that the hopping would occur in the adiabatic domain. The hopping instead will take place within the non-adiabatic control.

The experimental slopes did not match the predicted slopes, as can be seen from the plot of $\ln\sigma$ versus W at $T=450$ K in Fig. 8. For glasses and GCNs, the estimated temperatures (T_e) determined upon the experimental slopes seem to have been $T_e=470$ K and 663 K, accordingly, which are higher than the experimental temperature ($T=450$ K).

The least-square straight-line fittings of the results are shown in Fig. 9 beside the influence of BaTiO₃ concentration on the pre-exponential factors (σ_o), revealing a rise by increasing the BaTiO₃ percentage from 5 mol.% to

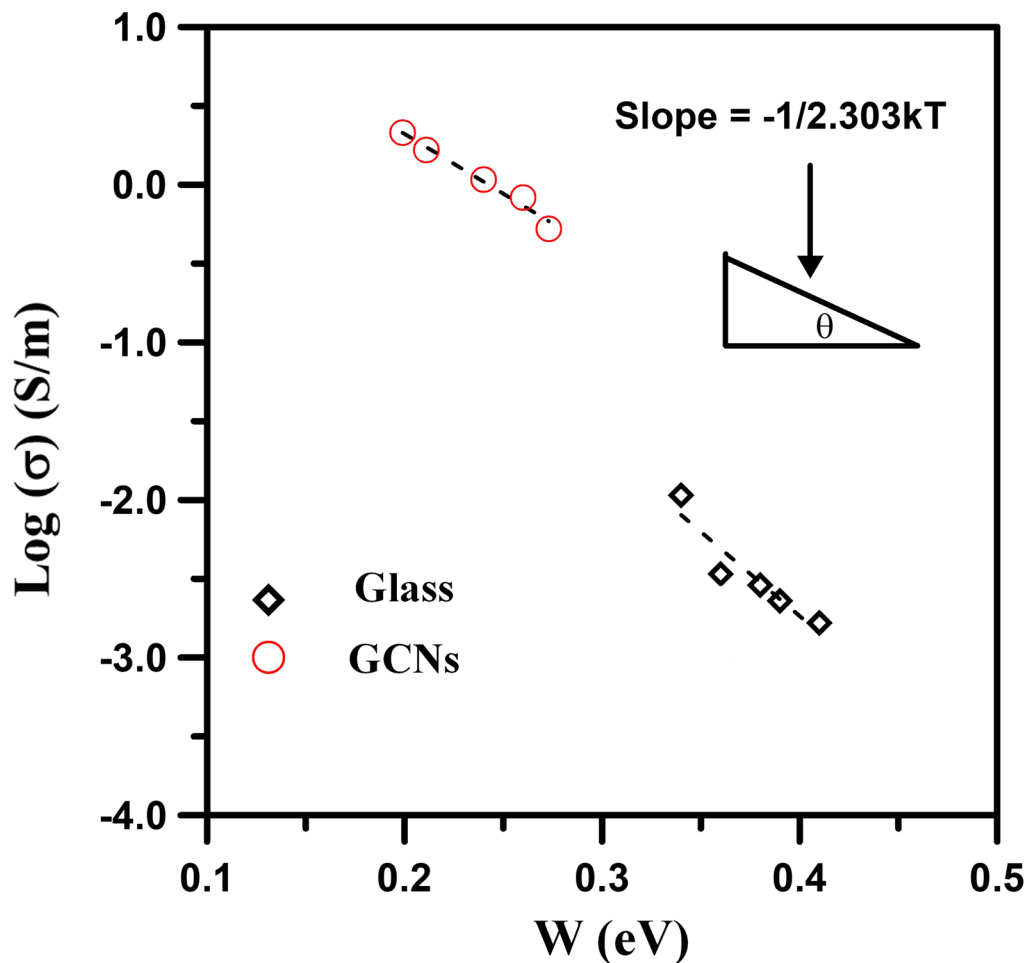


Fig. 8 DC conductivity (σ) at $T=450$ K for various glasses and GCNs as a function of activation energy (W).

25 mol.%. According to both findings, the polaron non-adiabatic hopping is the conduction mechanism in the current glass and GCNs.

Polaron Hopping Parameters

The approach suggested by Holstein³⁶ for estimating the polaron hopping energy W_H is as follows:

$$W_H = (1/4N)\Sigma_p [r_p]^2 \hbar \omega_p \quad (5)$$

where ω_p refers to the frequency of the optical phonons and $[r_p]^2$ is the electron–phonon coupling factor. The polaron radius, r_p , for a non-dispersive system of frequency ν_o for Eq. 6, on the other hand, was determined by Bogomolov et al.³⁷ as follows:

$$r_p = \left(\frac{\pi}{6}\right)^{1/3} \frac{R}{2} \quad (6)$$

For the current system, the values of the polaron radii obtained from Eq. 6 employing R listed in Tables I and II are displayed across the two tables. Whereas the previous computation ignored the potential impact of the disorder, the modest polaron radii values indicate that the polarons are extremely confined.

According to fundamental theories, the thermally activated electron hopping density of states close to the Fermi level is as follows:³⁸

$$N(E_F) = \left(\frac{3}{4}pR^3 W\right) \quad (7)$$

Tables I and II include the $N(E_F)$ values which refer to the localized states for the glasses and associated GCNs.

In the utilization of the experimental data in Tables I and II, we calculated the optical phonon frequency (ν_o) in Eq. 3 following the formula $k\theta_D = h\nu_o$ (h refers to the Planck constant).

At the point where the curve slope in Fig. 5a and b changed significantly, the Debye temperature θ_D was

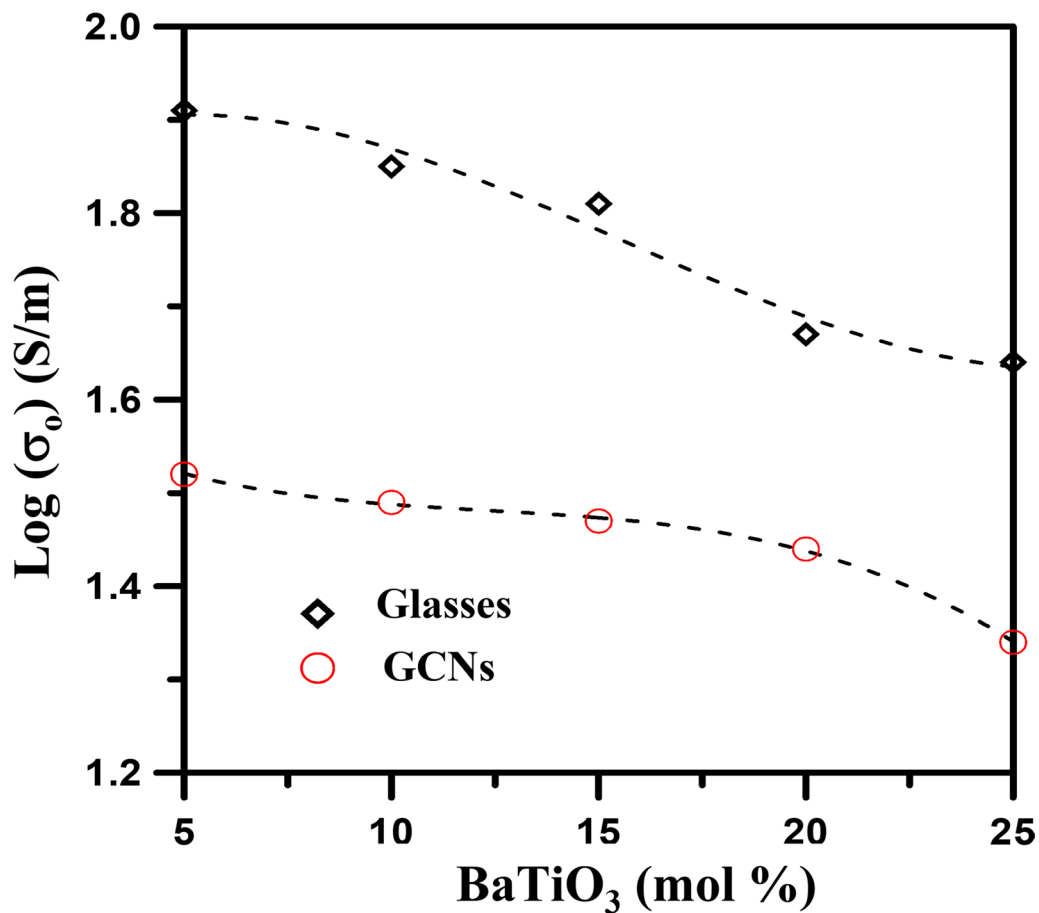


Fig. 9 Pre-exponential factor (σ_0) for various glasses and GCNs as a function of BaTiO₃ content.

calculated using the values listed in Tables I and II to determine ν_o for the various compositions.

For G and corresponding GCNs, the θ_D of the current system was found to be 615–645 K and 58–605 K, respectively. These values are comparable to those of the BaTiO₃-V₂O₅ and SrTiO₃-V₂O₅-PbO₂ glass systems. Therefore, these estimated θ_D values are considered reasonable. Then, ν_o was determined using the θ_D value. Tables I and II provide summaries of the values of θ_D and ν_o .

Conclusion

By annealing at crystallization temperature T_c , GCNs based on $x\text{BaTiO}_3-(80-x)\text{V}_2\text{O}_5-20\text{PbO}$ (where $x=5$ mol.%, 10 mol.%, 15 mol.%, 20 mol.%, and 25 mol.%) glasses were created. They are composed of tiny crystallites embedded in a glassy matrix after annealing. With a greater BaTiO₃ level, the crystallization temperature of T_c increases. The XRD and TEM results for GCNs demonstrate that nanocrystals with an average particle size of 50 nm were incorporated within the glassy matrix. Compared to the basic glasses,

the resultant materials have significantly increased electrical conductivity. It is assumed that the interstitial zone that developed between crystalline and amorphous phases is primarily responsible for the increased conductivity of these nanomaterials. These regions provide a greater concentration of V⁴⁺-V⁵⁺ pairs than within the glassy matrix, increasing the electron hopping. Appropriate amounts for different SPH variables are found utilizing optimal fits. The small polaron non-adiabatic hopping is mainly responsible for the electrical conductivity.

Funding Open access funding provided by The Science, Technology & Innovation Funding Authority (STDF) in cooperation with The Egyptian Knowledge Bank (EKB).

Data Availability Data will be made available on request.

Conflict of interest The authors declare that there is no conflict of interest in the current article.

Open Access This article is licensed under a Creative Commons Attribution 4.0 International License, which permits use, sharing, adaptation, distribution and reproduction in any medium or format, as long

as you give appropriate credit to the original author(s) and the source, provide a link to the Creative Commons licence, and indicate if changes were made. The images or other third party material in this article are included in the article's Creative Commons licence, unless indicated otherwise in a credit line to the material. If material is not included in the article's Creative Commons licence and your intended use is not permitted by statutory regulation or exceeds the permitted use, you will need to obtain permission directly from the copyright holder. To view a copy of this licence, visit <http://creativecommons.org/licenses/by/4.0/>.

References

1. V. Berbenni, A. Marini, and G. Bruni, Effect of mechanical milling on solid state formation of BaTiO₃ from BaCO₃-TiO₂ (rutile) mixtures. *Thermochim. Acta* 374, 151–158 (2001).
2. C. Beck, W. Härtl, and R. Hempelmann, Size-controlled synthesis of nanocrystalline BaTiO₃ by a sol-gel type hydrolysis in microemulsion-provided nanoreactors. *J. Mater. Res.* 13, 3174–3180 (1998).
3. S. Wei Lu, B.I. Lee, Z. Lin Wang, and W.D. Samuels, Hydrothermal synthesis and structural characterization of BaTiO₃ nanocrystals. *J. Cryst. Growth* 219, 269–276 (2000).
4. L. Lin, J. Huang, W. Yu, L. Zhu, H. Tao, P. Wang, Y. Xu, and Z. Zhang, Investigation of ferromagnetism in (Mn, Ga) co-doped LiNbO₃ by density functional theory. *J. Magn. Magn. Mater.* 500, 166380 (2020).
5. M.S. Al-Assiri, M.M. El-Desoky, A. Al-Hajry, A. Al-Shahrani, A.M. Al-Mogeeth, and A.A. Bahgat, Study of nanostructural behavior and transport properties of BaTiO₃ doped vanadate glasses and glass-ceramics dispersed with ferroelectric nanocrystals. *Phys. B* 404, 1437–1445 (2009).
6. N. Syam Prasad and K.B.R. Varma, Evolution of ferroelectric LiNbO₃ phase in a reactive glass matrix (LiBO₂-Nb₂O₅). *J. Non-Cryst. Solids* 351(16–17), 1455–1465 (2005). <https://doi.org/10.1016/j.jnoncrsol.2005.03.040>.
7. Y. Hu and C.L. Huang, Crystallization kinetics of the LiNbO₃-SiO₂-Al₂O₃ glass. *J. Non-Cryst. Solids* 278, 170–177 (2000).
8. M. Todorović and L. Radonjić, Lithium-niobate ferroelectric material obtained by glass crystallization. *Ceram. Int.* 23, 55–60 (1997).
9. M.M. El-Desoky, I. Morad, H.E. Ali, and F.A. Ibrahim, Structure analyses and ferroelectric behaviour of barium titanate-doped glass-ceramic nanocrystals for energy storage applications. *Appl. Phys. A* 129, 196 (2023).
10. H.C. Zeng, K. Tanaka, K. Hirao, and N. Soga, Crystallization and glass formation in 50Li₂O-50Nb₂O₅ and 25Li₂O-25Nb₂O₅-50SiO₂. *J. Non-Cryst. Solids* 209, 112–121 (1997).
11. J.M. Ziman, *Electrons and Phonons: The Theory of Transport Phenomena in Solids* (Oxford University Press, 2001).
12. I. Bakonyi, Accounting for the resistivity contribution of grain boundaries in metals: critical analysis of reported experimental and theoretical data for Ni and Cu. *Eur. Phys. J. Plus* 136, 410 (2021).
13. M.M. El-Desoky, F.A. Ibrahim, A.G. Mostafa, and M.Y. Hassan, Effect of nanocrystallization on the electrical conductivity enhancement and Mössbauer hyperfine parameters of iron based glasses. *Mater. Res. Bull.* 45, 1122–1126 (2010).
14. J.E. Garbarczyk, P. Jozwiak, M. Wasiucioneck, and J.L. Nowinski, Nanocrystallization as a method of improvement of electrical properties and thermal stability of V₂O₅-rich glasses. *J. Power Sources* 173, 743–747 (2007).
15. A.A. Bahgat, On the ferroelectricity of Bi-cuprate glass doped with K ions. *Phys. Status Solidi (A)* 200(1), R1–R4 (2003). <https://doi.org/10.1002/pssa.200309015>.
16. M.M. El-Desoky, Giant electrical conductivity enhancement in BaO-V₂O₅-Bi₂O₃ glass by nanocrystallization. *Mater. Chem. Phys.* 119, 389–394 (2010).
17. K. Saito, Material creation by high temperature processing. *Materia* 50(3), 116–119 (2011).
18. J.E. Garbarczyk, P. Jozwiak, M. Wasiucioneck, and J.L. Nowinski, Effect of nanocrystallization on the electronic conductivity of vanadate-phosphate glasses. *Solid State Ion.* 177, 2585–2588 (2006).
19. N.K. Wally, E. Sheha, B.M. Kamal, A.E. Hannora, and M.M. El-Desoky, Exploring the electrochemical properties of Na₂S-V₂O₅-P₂O₅ glass-ceramic nanocomposites as a cathode for magnesium-ion batteries. *J. Alloy. Compd.* 895, 162644 (2022).
20. A. Al-Shahrani, A. Al-Hajry, and M.M. El-Desoky, Non-adiabatic small polaron hopping conduction in sodium borate tungstate glasses. *Phys. Status Solidi (A)* 200, 378–387 (2003).
21. W. Li, J. Shi, K.H.L. Zhang, and J.L. MacManus-Driscoll, Defects in complex oxide thin films for electronics and energy applications: challenges and opportunities. *Mater. Horizons* 7(11), 2832–2859 (2020). <https://doi.org/10.1039/D0MH00899K>.
22. I.G. Austin and N.F. Mott, Polarons in crystalline and non-crystalline materials. *Adv. Phys.* 18, 41–102 (1969).
23. N.F. Mott, Conduction in glasses containing transition metal ions. *J. Non-Cryst. Solids* 1, 1–17 (1968).
24. M.M. El-Desoky, H.S.S. Zayed, F.A. Ibrahim, and H.S. Ragab, Electrical conductivity improvement of strontium titanate doped lead vanadate glasses by nanocrystallization. *Phys. B* 404, 4125–4131 (2009).
25. M.S. Al-Assiri, S.A. Salem, and M.M. El-Desoky, Effect of iron doping on the characterization and transport properties of calcium phosphate glassy semiconductors. *J. Phys. Chem. Solids* 67, 1873–1881 (2006).
26. M.M. El-Desoky and M.S. Al-Assiri, Structural and polaronic transport properties of semiconducting CuO-V₂O₅-TeO₂ glasses. *Mater. Sci. Eng., B* 137, 237–246 (2007).
27. K.A. Mahmoud, O.L. Tashlykov, M.I. Sayyed, and E. Kavaz, The role of cadmium oxides in the enhancement of radiation shielding capacities for alkali borate glasses. *Ceram. Int.* 46, 23337–23346 (2020).
28. S.P. Dalawai, T.J. Shinde, A.B. Gadkari, N.L. Tarwal, J.H. Jang, and P.N. Vasambekar, Influence of Sn⁴⁺ on structural and DC electrical resistivity of Ni-Zn ferrite thick films. *J. Electron. Mater.* 46, 1427–1438 (2017).
29. M.M. El-Desoky and A. Al-Shahrani, Mixed electronic-ionic conductivity in semiconducting CaO-PbO-Fe₂O₃-P₂O₅ glasses. *Phys. B* 371, 95–99 (2006).
30. A. Al-Hajry, A. Al-Shahrani, and M.M. El-Desoky, Structural and other physical properties of barium vanadate glasses. *Mater. Chem. Phys.* 95, 300–306 (2006).
31. M.M. El-Desoky, DC conductivity and hopping mechanism in V₂O₅-B₂O₃-BaO glasses. *Phys. Status Solidi (A)* 195(2), 422–428 (2003). <https://doi.org/10.1002/pssa.200305944>.
32. F.A. Ibrahim, Electrical conductivity enhancement of V₂O₅-P₂O₅-Bi₂O₃ glasses by nanocrystallization. *J. Electron. Mater.* 51, 621–625 (2022).
33. S. Sakka and J.D. Mackenzie, Relation between apparent glass transition temperature and liquids temperature for inorganic glasses. *J. Non-Cryst. Solids* 6, 145–162 (1971).
34. T.K. Pietrzak, J.E. Garbarczyk, I. Gorzkowska, M. Wasiucioneck, J.L. Nowinski, S. Gierlotka, and P. Jozwiak, Correlation between electrical properties and microstructure of nanocrystallized V₂O₅-P₂O₅ glasses. *J. Power Sources* 194, 73–80 (2009).
35. M.S. Al-Assiri and M.M. El-Desoky, Nanocrystallization as a method of improvement of electrical properties of

- Fe₂O₃-PbO₂-TeO₂ glasses. *J. Mater. Sci. Mater. Electron.* 25, 3703–3711 (2014).
36. T. Holstein, Studies of polaron motion. *Ann. Phys.* 8(3), 343–389 (1959). [https://doi.org/10.1016/0003-4916\(59\)90003-X](https://doi.org/10.1016/0003-4916(59)90003-X).
37. V.N. Bogomolov, E.K. Kudinov, and Y.A. Firsov, Polaron nature of current carriers in rutile (TiO₂). *Soviet Phys. Solid State USSR* 9(11), 2502 (1968).
38. N. Mott, and F. Davis, *Electronic Processes in Non-Crystalline Materials* (Oxford: Clarendon Press, 1960), p.237.

Publisher's Note Springer Nature remains neutral with regard to jurisdictional claims in published maps and institutional affiliations.